Spider Monkey Metaheuristic Tuning of Model Predictive Control with Perched Landing Stabilities for Novel Auxetic Landing Foot in Drones

Magesh M[1], P.K. Jawahar[2,*], Saranya S.N.[3], Raj Jawahar R[4]
[1]Department of Aerospace Engineering, B. S. Abdur Rahman Crescent Institute of Science and Technology, Chennai, India
[2]Department of Electronics and Instrumentation Engineering, B. S. Abdur Rahman Crescent Institute of Science and Technology, Chennai, India
[3]Department of Electronics and Communication Engineering, Dayananda Sagar Academy of Technology and Management, Bangalore, India
[4]Department of Mechanical Engineering, Chennai Institute of Technology, Chennai, India
mageshm@crescent.education; [*]jawahar@crescent.education; saranya-ece@dsatm.edu.in; dynamechz.raj65@gmail.com

***Abstract*—The study focuses on improving drone landing gear dynamics through an innovative auxetic foot design, leveraging Spider Monkey Optimization for Model Predictive Control adjustment, facilitated by an Arduino-MATLAB interface. The auxetic foot design incorporates materials with a negative Poisson ratio, which allows the foot to expand and enhance energy absorption during landings. This design improves stability and safety during the perched landing process. The SMO-MPC approach is used to optimise the control of the perched landing gear. SMO, inspired by spider monkey search behaviour, optimises auxetic foot control input sequences with the limits of rotational displacement (theta = 30 deg to -30 deg) on the prediction horizon to improve landing gear performance. The real-time implementation of SMO-MPC is achieved through an Arduino-MATLAB interface on quadcopter drone. A comparative analysis is conducted to evaluate the benefits of SMO-MPC compared to conventional MPC methods. The results show that the SMO-MPC approach with auxetic foot design surpasses conventional MPC methods in terms of landing performance with 14.6 % improvement in damping force control and control of aerodynamic stability with pitch of 34.16 %, yaw of 16.87 %, and roll of 31.74 %.**

***Index Terms*—Metaheuristic optimisation; Spider monkey optimisation; Unmanned aerial vehicle; MPC; SMO-MPC.**

I. INTRODUCTION

Perched landing with bird-like manoeuvres offers advantages such as reduced footprint, enhanced stability, and increased manoeuvrability for drones. It allows them to land in urban environments with limited space, maintain stability under challenging conditions, and navigate through tight spaces with ease [1]. Perched landing environments offer a range of applications for unmanned aerial vehicles (UAVs). These applications include surveillance and security, inspection and maintenance of tall structures, environmental monitoring, precision agriculture, search and rescue operations, filmmaking and photography, and scientific research in biology, ecology, and wildlife studies. Perched landing UAVs can access elevated perches, enabling them to capture high-resolution imagery, collect data, and provide valuable aerial perspectives in areas that humans may be difficult to reach. These UAVs are used in all industries to improve situational awareness, optimise farming practices, monitor environmental conditions, aid in search and rescue missions, capture unique shots for entertainment purposes, and study wildlife behaviour without disturbing natural habitats.

Perched landing for drones presents challenges such as precise localisation, sensing and perception, control in unstructured environments, wind and environmental conditions, dynamic perch movements, and leg design and control. These challenges require precise localisation, perception techniques, adaptation to uneven surfaces, and dynamic perch movements to ensure safe and accurate landings. Drones rely on communication and navigation systems to control the flight path and landing. Any disruption or failure in these systems can make it difficult to control and land UAVs. You must avoid obstacles during flight, such as trees, buildings, and other UAVs, which can make it difficult to control and land them safely [2]. Perched landings require leg kinematics, force control, safety, real-time timing, system complexity, and validation. Iterative design, rigorous testing, and continuous improvement are crucial for successful landings [3].

To address these challenges, various technologies and approaches have been developed to improve UAV stability and landing capabilities. For example, some UAVs are equipped with sensors and algorithms that can detect wind conditions and adjust their flight path to maintain stability. Additionally, some UAVs use advanced control systems and

Manuscript received 10 June, 2023; accepted 25 January, 2024.

machine learning algorithms to optimise their flight path and landing trajectory [4], [5]. In addition, some UAVs use advanced landing systems, such as parachute landing systems or landing gear, to ensure a safe and controlled landing. Overall, stability and landing of UAVs are critical challenges that must be addressed to ensure safe and efficient UAV operations. Advances in technology and innovation will continue to improve UAV capabilities and enhance their stability and landing capabilities.

Different types of landing gear are used depending on the size, purpose, and intended operating environment of the drone. Retractable or adjustable landing gear allows for unobstructed shots or videos with increased aerodynamic efficiency which is discussed by Huang in [6]. Liang, Chin, Sun, and Wang [7] implemented skid landing gear in UAV because of its lightweight and suitability for confined spaces. Campi, Cruciani, Maradei, and Feliziani [8] studied the dynamics of fixed landing gear in larger drones for rough terrains and found that landing of UAVs on flat surfaces is stable than on rough terrains. Articulated landing gear used by Ni, Yin, Wei, Zhong, and Nie [9] offers flexibility and shock absorption on uneven surfaces, whereas the sprung landing gear proposed by Bauer [10] absorbs shocks and protects sensitive equipment such as a camera mounted on the UAV.

The limitations of landing gear depend on factors such as drone size, weight, control of gyroscopic moments, landing velocity, damping force and altitude, land surface complexity, and wind velocity. The landing gears of the quadcopter reveal various studies aimed at optimising design, materials, and structure to improve performance. Some studies by Cheng and Matsuoka focussed on stability and impact resistance, while others proposed deployable systems to absorb impact forces and reduce damage [11]. Jia, Jizhen, Xiaochuan, and Yazhou [12] explored landing gear designs and models for UAVs, covering configurations, materials, shock absorption mechanisms, and modelling techniques. Chu, Guo, and Xing [12] discussed the design and development of a foldable system for a quadrotor UAV that evaluated performance. Chen, Zhao, Zhang, and Zhu [14] proposed a UAV that uses dynamic simulation for optimal design and control. Ikura, Miyashita, and Ishikawa [15] studied the severity of UAV collisions with UAV structures, providing insight into the influence of various parameters on the impact force. Muskardin *et al.* [16] assessed operational safety to avoid collision by improving UAV safety assessment practices. The paper discusses impact forces during landing and the effects of design parameters on overall performance.

From the above survey, there is a need to obtain the control stabilities of drones, which involves a metaheuristic landing approach like-bird manoeuvres. The auxetic landing gear is an innovative type of drone landing gear that uses unique mechanical properties with a negative poisson ratio [17]. These materials offer potential benefits such as impact absorption, load distribution, versatility, weight reduction, compact storage, and vibration damping [18]. However, research and development is ongoing, requiring careful engineering, material selection, structural design, and manufacturing processes. Further research is needed to evaluate long-term durability, fatigue resistance, and real-world performance in various environmental conditions and operational scenarios.

Model predictive control (MPC) is a robust technique for drone landing control due to its dynamic optimisation, handling limitations, real-time modifications, and precise landings [19]. Research articles highlight the advantages of MPC-based techniques for autonomous and quadrotor UAVs, focussing on system dynamics, cost functions, and control methods [20]. The use of wind-aware control methods and nonlinear MPC for precision landing in wind-disturbed conditions is also explored in [21], [22]. Traditional optimisation methods face limitations in solving complex problems [23]. They can be slow to converge, especially for high-dimensional problems, and may converge to local optima instead of the global optimum. Computational costs can be significant for large-scale problems, making them impractical for real-world applications [24], [25]. Additionally, traditional optimisation methods struggle to handle with nonlinear functions, which can be unstable and unreliable.

To address these limitations, metaheuristic optimisation methods such as spider monkey optimisation (SMO) were applied to MPC. SMO-based MPC offers advantages such as exploring the entire search space, reducing computing time, ensuring robustness, and adapting to different optimisation issues and control objectives. The proposed work with MPC-based SMO optimisation for controlling novel auxetic landing foot with perched landing mechanism provides an effective solution for drone landing control, overcoming the limitations of traditional methods and delivering enhanced aerodynamics and landing stability in challenging conditions.

II. QUADCOPTER MODELLING

A. Modelling of the Quadcopter Drone

The system dynamics of the quadcopter was modelled using Newton-Euler theory based on the aerodynamic stability criterion with state-space representation as second-order model [26]:

$$\ddot{a} = \left(\cos r \sin p \cos y + \sin r \sin y\right)\frac{f_1}{m} + D_a, \tag{1}$$

$$\ddot{b} = \left(\cos r \sin p \cos y + \sin r \sin y\right)\frac{f_1}{m} + D_b, \tag{2}$$

$$\ddot{c} = \left(\cos r \cos p\right)\frac{f_1}{m} + D_c, \tag{3}$$

$$\ddot{r} = \dot{p}\dot{y}\frac{I_b - I_c}{I_a} + \frac{J_r}{I_a}\dot{p}S_r + \frac{l}{I_a}f_2 + D_r, \tag{4}$$

$$\ddot{p} = \dot{y}\dot{r}\frac{I_c - I_a}{I_b} + \frac{J_r}{I_b}\dot{r}S_r + \frac{l}{I_b}f_3 + D_p, \tag{5}$$

$$\ddot{y} = \dot{r}p\frac{I_a - I_b}{I_c} + \frac{l}{I_c}f_4 + D_y, \tag{6}$$

where (a, b, c) represent the centre of gravity of the UAV in the earth frame; (u, v, w) represent the angular velocity of the body frame; the total mass of the UAV, m, is multiplied by the acceleration of gravity, g; the arm length of the UAV is denoted by l; I_a, I_b, and I_c stand for the moments of inertia; r, p, and y signify the roll, pitch, and yaw Euler angles,

respectively; J_r stands for the moment of inertia; D_a, D_b, D_c, D_r, D_p, and D_y stand for disturbances; the i^{th} propeller speed, S_i (i = 1, 2, 3, 4), and the total propeller speed, $S_r = S_1 \times S_2 + S_3 \times S_4$, are both expressed in m/s.

B. UAV Landing Gear Model

Assuming that the UAV uses a perching method to landing, we can expect that its entire leg and foot system will behave like a flexible body. Thus, the UAV system's flight dynamics are captured using a quadcopter model, as illustrated in Figure 1, with position and orientation described by the tuple (P, Q) and a specific slant angle predetermined. To ignore gravity and achieve static equilibrium, we set p = 0 and q = 0. Just pretend there is no auxetic dampening and use a linear spring. The suspension model for UAV landing gear dynamics is described as follows:

$$e_2(q-p) = F_{s2}; \quad F_d = b(\dot{q}-\dot{p}), \tag{7}$$

$$F_{s1} = e_1(p-u), \tag{8}$$

$$\sum F = ma. \tag{9}$$

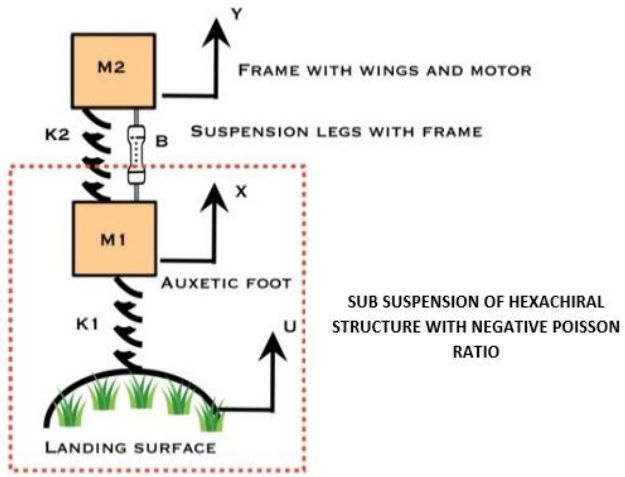

Fig. 1. Schematic representation of the dynamical model of the system.

Mass 2:

$$\begin{bmatrix} \sum F = -F_{s2} - F_d = m_2\ddot{q} \\ -e_2(q-p) - b(\dot{q}-\dot{p}) = m_2\ddot{q} \end{bmatrix}. \tag{10}$$

Mass 1:

$$\begin{bmatrix} \sum F = -F_{s2} - F_d - F_{s1} = m_1\ddot{p} \\ e_2(q-p) - b(\dot{q}-\dot{p}) - e_1(p-u) = m_1\ddot{p} \end{bmatrix}, \tag{11}$$

$$\begin{bmatrix} m_1\ddot{p} + b\dot{p} + (e_1+e_2)p = b\dot{q} + e_2q + e_1u \\ m_2\ddot{q} + b\dot{q} + e_2q = b\dot{p} + e_2x \\ m_2\dfrac{d^2q}{dt^2} + b\dfrac{dq}{dt} + e_2q = b\dfrac{dp}{dt} + e_2p \end{bmatrix}, \tag{12}$$

where m_1- mass of auxetic foot; m_2 - mass of the frame with wings and motor; e_1 - subsuspension of hexachiral structure with negative Poisson ration; e_2 - suspension of leg with frame; b - damping coefficients. Taking the Laplace transform to find transfer function,

$$\begin{bmatrix} L\left(\dfrac{d^2q}{dt^2}\right) = s^2Q(s) - sq(0) - \dfrac{dq(0)}{dt} \\ L\left(\dfrac{dq}{dt}\right) = sQ(s) - q(0) \\ L(q(t)) = Q(s) \\ L\left(\dfrac{dp}{dt}\right) = sP(s) \\ L(p(t)) = P(s) \\ m_2s^2Q(s) + bsQ(s) + e_2Q(s) = bsP(s) + e_2P(s) \end{bmatrix}, \tag{13}$$

$$\begin{bmatrix} Q(s)\lfloor m_2s^2 + bs + e_2 \rfloor = P(s)[bs + e_2] \\ \dfrac{Q(s)}{P(s)} = \dfrac{bs+e_2}{m_2s^2 + bs + e_2} \end{bmatrix}. \tag{14}$$

The second consideration is with rotary model of the auxetic foot during perched landing. Coordinates (r) and the orientation are defined; assume linear spring and damper parameters are lumped together (Fig. 2):

$$b\dot{r} = T_dT_s = kr, \tag{15}$$

$$\sum M = J\alpha, \tag{16}$$

$$\sum M = T - T_d - T_s = J\ddot{r}, \tag{17}$$

$$\begin{bmatrix} T = br - kr = J\ddot{r} \\ J\ddot{r} + b\dot{r} + kr = T \end{bmatrix}, \tag{18}$$

where $k = k_1 + k_2$.

$$J\frac{d^2r}{dt^2} + b\frac{dr}{dt} + kr = T(t). \tag{19}$$

b is the damping coefficient of the leg, k is the stiffness of the leg, and θ is the angular displacement of the foot.

Taking the Laplace transform to find transfer function,

$$\begin{bmatrix} L\left(\dfrac{d^2r}{dt^2}\right) = s^2R(s) - sr(0) - \dfrac{dr(0)}{dt} \\ L\dfrac{dr}{dt} = sR(s) - r(0) \\ L(r(t)) = R(s) \\ L(T(t)) = T(s) \\ T(s) = Js^2R(s) + bsR(s) + kR(s) \end{bmatrix}, \tag{20}$$

$$\frac{R(s)}{T(s)} = \frac{1}{Js^2 + bs + k}, \tag{21}$$

where J is the polar moment of inertia between the auxetic foot and ground, $\frac{d^2r}{dt^2}$ is the angular acceleration of auxetic foot, and $\frac{dr}{dt}$ is the angular velocity of auxetic foot as shown in equation 20.

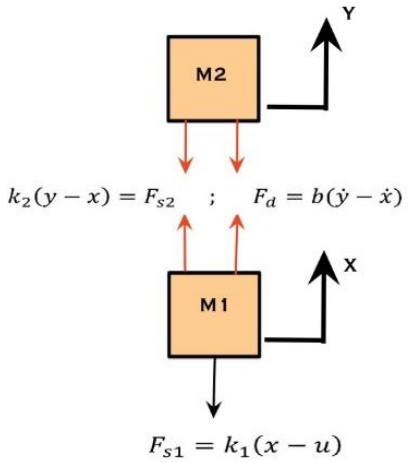

Fig. 2. Schematic representation of the system landing gear model.

III. Model Predictive Control

The specific implementation of a model predictive control (MPC) algorithm for landing gear control on a drone will depend on the particular system being controlled and the desired outcome [27]. However, here is a general outline of the steps involved in designing an MPC algorithm for landing gear control:

– The mathematical model of the drone dynamics and the landing gear mechanism are developed based on factors such as the drone weight, size, and aerodynamics, as well as the characteristics of the landing gear, such as its length, stiffness, and damping;

– State and control inputs for the MPC algorithm: The state variables include the drone position, velocity, and orientation, as well as the position and orientation of the landing gear. The control inputs may include the position and orientation of the landing gear actuators;

– The objective function for the MPC algorithm: This function should specify the desired outcome of the landing process, such as minimising the impact force on the drone, and should be a function of the state variables and control inputs;

– Set the prediction and control horizons for the MPC algorithm, which determine the optimal control input based on the predicted system behaviour and the objective function. Implement the algorithm by solving optimisation problems at each time step. Test and validate the algorithm in simulation and real-world conditions, refining the model and algorithm as needed;

– The following is an illustration of the objective function

$$Q=\sum_{i=1}^{P_h} a_i\left(q'\left(t+i|t\right)-b\left(t+i\right)\right)^2+ \\ +\sum_{i=1}^{C_h} c_i\left(e\left(t+i\right)-e\left(t+i-1\right)\right)^2, \quad (22)$$

where P_h is the time span predicted, C_h is the time span controlled, a_i and c_i are weighting coefficients, etc. The restrictions are as follows, where $\acute{q}(t+i|t)$, $b(t+i)$, $and\ e(t+i)$ represent the expected output, the desired output, and the next control signal, respectively:

$$p\left(t+1\right)=f\left(p\left(t\right),e\left(t\right)\right), \quad (23)$$

$$q\left(t\right)=g\left(p\left(t\right),e\left(t\right)\right), \quad (24)$$

$$e_l\le\left\|e\left(t\right)\right\|\le e_u, \quad (25)$$

$$p_l\le\left\|p\left(t\right)\right\|\le p_u. \quad (26)$$

Here, e_l, e_u denote the minimum and maximum controllable signals, and p_l, p_u the minimum and maximum allowable system states.

IV. Spider Monkey Optimisation (SMO)

Spider monkey optimisation (SMO) is an optimisation technique inspired by the natural world. It involves spider monkeys exploring and exploiting search spaces to find the best solution. SMO is comparable to other advanced algorithms, such as particle swarm optimisation and genetic algorithms, in terms of solution quality and convergence time [28]. However, it requires refinement and validation to ensure its reliability and efficiency for specific optimisation problems.

Spider Monkey Optimisation-Based Model Predictive Control (SMO-MPC). SMO can be used with MPC to optimise the control parameters of a drone's landing gear system. The goal is to achieve a stable and smooth landing of the drone by optimising the control parameters of the landing gear system.

The process of combining SMO and MPC for drone landing stability and landing gears can be broken down into the following steps: A mathematical model of a drone landing system should consider factors such as mass, velocity, position, terrain, and wind conditions. Optimise the cost function using SMO using control parameters and reflect the desired drone behaviour [29]. Initialise a spider monkey population with random control parameters to represent candidate solutions.

Initialisation. To optimise for a set of control variables, SMO creates a population with uniform distribution in [m and c], where m is the number of monkeys and c is the number of control variables. The equation is used to initialise each monkey

$$SM_{ab}=SM_{\min b}+\left(SM_{\max b}-SM_{\min b}\right)\times U\left(0,1\right), \quad (27)$$

where SM_{maxb} and SM_{minb} represent the maximum and minimum values for the monkey in the b^{th} direction, respectively, and U(0, 1) is a uniformly distributed random number between 0 and 1.

Local Leader Phase (LLP). At this stage, monkeys update their present position based on the knowledge of their local leader and group members, a strategy that is mainly used for search. The position of the g^{th} local group monkey (a^{th} monkey) is updated using the equation below. It is important to select an appropriate perturbation rate (pr) because it determines the magnitude of the shift from the current position

$$SM_{newab}=SM_{ab}+\left(LL_{gb}-SM_{ab}\right)\times U\left(0,1\right)+ \\ +\left(SM_{fb}-SM_{ab}\right)\times U\left(-1,1\right), \quad (28)$$

where SM_{ab} is the b^{th} dimension of the a^{th} monkey, LL_{gb} is the

b^{th} dimension of the g^{th} place in the local group leadership hierarchy, U(-1, 1) is an arbitrary number in the range of [-1, 1], SM_{fb} is the b^{th} dimension of the f^{th} monkey selected at random within the g^{th} group such that f is not equal to a.

Global Leader Phase (GLP). Exploitation is the primary goal of the global leader phase, during which all monkeys update their positions based on what they have learnt from the global leader and their fellow group members at the local level. The position is updated using the equation represented

$$SM_{newab} = SM_{ab} + \left(GL_{gb} - SM_{ab}\right) \times U\left(0,1\right) + \\ + \left(SM_{fb} - SM_{ab}\right) \times U\left(-1,1\right), \quad (29)$$

where GL_b stands for the "global leader in dimension b". Equation uses a variable called probabilities (prb_a) to update the location of the a^{th} monkey precisely

$$prb_a = 0.1 + \left(\frac{fit_a}{fit\max}\right) \times 0.9, \quad (30)$$

fit_a denotes the fitness value of the a^{th} monkey, and the highest value among them is denoted by fitmax. Thus, fitter monkeys are more likely to have a higher probability of having their positions updated.

Local Leader Learning (LLL) phase. Here, the greedy selection algorithm is used to determine the new local leader (the monkey with the highest fitness). The local limit count is increased by one if the local leader position is not updated.

Global Leader Learning (GLL) phase. During this stage, the current global leader is determined through greedy selection. The global limit count is then increased by one if the new position is not an update from the previous global leader position.

Local Leader Decision (LLD) phase. If the local leader is not changed within a given number of iterations (the "local leader limit"), then all members of the group will be reset to their initial states. Each member of that group can be initialised in one of two ways: at random or by combining data from the group's local leader and global leader via an equation

$$SM_{newab} = SM_{ab} + \left(GL_{gb} - SM_{ab}\right) \times U\left(0,1\right) + \\ + \left(SM_{ab} - LL_{gb}\right) \times U\left(0,1\right). \quad (31)$$

The formula mentioned above demonstrates that an upgraded monkey dimension is drawn to a global leader and repulsed by a local leader. The fitness of spider monkey is evaluated using the MPC algorithm, simulating drone landings and controlling parameters. Best-performing spider monkeys are validated using heuristics to generate new values of control parameters.

Global Leader Decision (GLD) phase. In this stage, the global leader recombines the entire population into a single group, then divides it into a smaller number of groups (beginning with two, then three, etc.) if the global leader position remains unaltered for a certain number of trials (= global leader limit).

Steps 4 and 5 are repeated until the convergence criterion is met. Use optimised control parameters in the MPC algorithm to control the landing gear system. SMO-based MPC improves stability, safety and reduces impact force, prolonging the life of the system.

V. REAL-TIME IMPLEMENTATION

Quadcopters consist of four rotors, a frame, batteries, and a controller (Fig. 3). They are designed to be lifted and steerable, with rotors supporting the rotors and components. The quadcopter model involves lift, propulsion, and control, while dynamic models simulate flying and landing. Perching on hind legs requires force control, kinematics, sensing (distance between ground d), perception, and control algorithms. The leg design must provide enough forces and torques to support the robot's mass, position, and orientation. The landing gear foot in this case is shaped of auxetic material that functions as a contact module; this is necessary for the development of a flexible auxetic foot (rf, lf). The interface of the landing gear with the ground is passively stabilised by these modules, while the dynamic load of landing (damping force Fd) is absorbed by an auxetic foot of hexachiral design. Fusion deposition techniques are used to create a 3D thermally resistant filament rubber polyurethane with grid layers for auxetic landing gear. Furthermore, the designs are in accordance with the geometrical characteristics of the contact areas (Fig. 4); however, there is always a discrepancy between the designed contact module and the actual contact surfaces. To reduce the impact difference and improve contact stability, the proposed contact module is made of soft materials. Similarly, to fractals, auxetic structures are made by repeatedly replacing a single edge at progressively smaller increments. The wall edges deviate from the vertical plane by an amount determined in large part by the oblique angle

$$0 \le \sum_{m=1}^{i} \Upsilon_m \le 0.5. \quad (32)$$

For a first-order, 30 °-angled hexachiral, the wall thickness is

$$t_f = \frac{t_r}{1+2\Upsilon}. \quad (33)$$

The F_i, or mean compressive impact force during landing, is calculated by

$$F_i = \frac{89.6}{K} \sigma L_O^{0.5} t_o^{1.5}. \quad (34)$$

Roll (r), pitch (p), and yaw (y) angles characterise the rotating motion of an aircraft or spacecraft. Pitch is the attitude angle, while roll is the longitudinal axis rotation. Yaw regulates horizontal motion, pitch - vertical. These angles describe the three-dimensional orientation and rotation of an object. Roll, pitch, and yaw angles (φ, θ, ψ) can modify the orientation and horizontal motion of the object.

Geometry and optimisation calculate leg trajectories, while impact-resistant legs have compliance and stabilisation systems. Safety features such as detection, avoidance, and response to danger are difficult to create.

Simulation and real-world testing are necessary to trust robotic leg control algorithms. Lightweight RC servos can

control the perched legs of drones, considering landing pressures, weight, and range of motion. Real-time sensors measure leg placement and force, and failsafe systems and emergency stop switches are necessary for safety. Test and experimental validation are necessary to ensure stability and control settings.

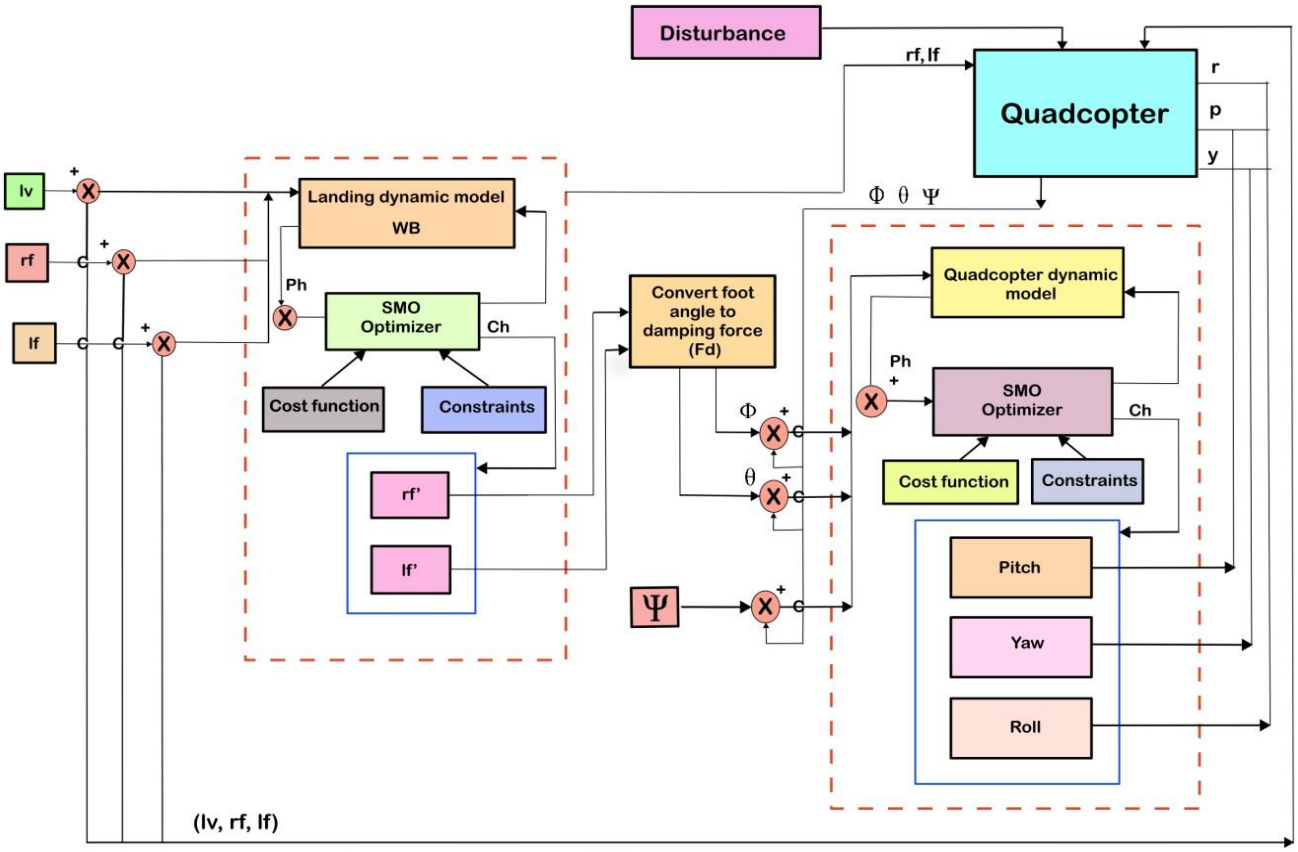

Fig. 3. Proposed quadcopter drone controller schematics.

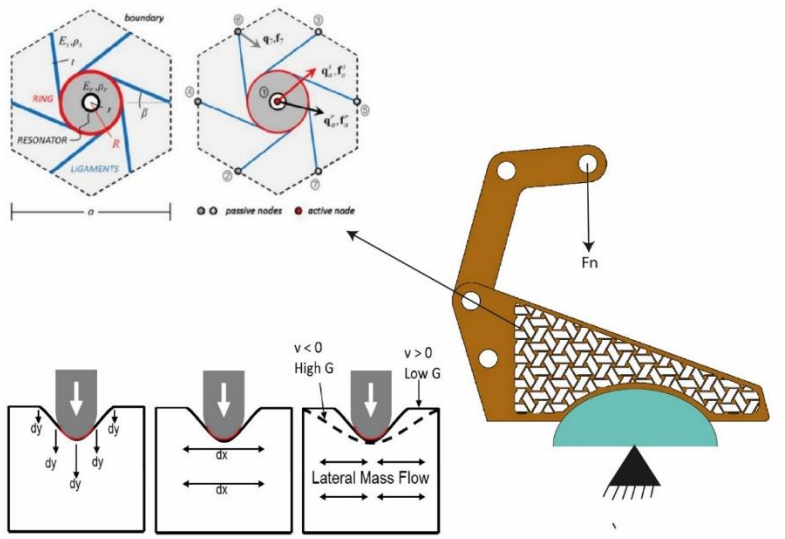

Fig. 4. Schematics and mechanism of the auxetic landing gear.

The real-time drone control mechanism consists of several key components and software tools (Fig. 5).

The ATMega328P controller serves as the central control unit, receiving commands and controlling the flight of the drone. The NRF24L01 communication module enables long-range wireless communication between the drone and the ground station. The GPSNeo6M GPS module provides accurate global positioning data for autonomous navigation. The HMC5883L magnetometer determines the drone's heading, while the MPU6050 gyro and accelerometer provide orientation and position data. The RC servo with 35 kg torque controls the landing gear position, and the BMP180 barometric sensor measures altitude as shown in Table I. MultiWii software facilitates drone control, and MATLAB is used to implement model predictive control (MPC) algorithms to optimise flight parameters. Together, these components and software enable precise control, autonomous navigation, stability, and advanced features such as altitude hold and waypoint tracking. The integration of MPC enhances responsiveness and adaptability, ensuring safe and

efficient drone operations.

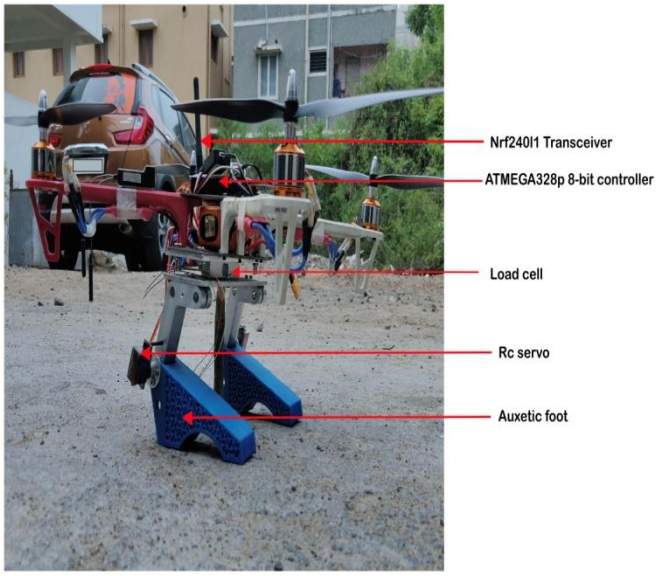

Fig. 5. Phtotographic view: Drone with auxetic foot.

VI. RESULTS AND DISCUSSION

The SMO algorithm is customised with the following settings: Maximum iterations = 1000, population size = 30, global leader limit = 125, local leader limit = 150, maximum groups = 30, and maximum perturbation rate = 0.21 over time. 50 iterations of the optimisation were performed and the best result was selected as the optimal parameters of the controller.

TABLE I. OPERATING PARAMETERS AND CONDITIONS.

Parameters	Value
Drone system	
Motor type	Brushless D.C. motor
No. of motors	4
GPS	GPSNeo6M
IMU	MPU6050
Magnetic Compass	HMC5883L
Altitude Sensor	BMP180
Auxetic gripper	
Material	Thermo resistive polyurethane rubber
Type	Hexachiral
Max. negative Poisson's ratio	-0.00247
Max. deformation (mm)	41.6
Load cell sensor	
Type	S-Bridge type
Range	-200 KN to 850 KN
Sensitivity	0.1 KN to 1 KN
Output	4 mA–20 mA
Displacement sensor	
Type	Hall effect
Range	0 mm–100 mm
Sensitivity	0.5 V ± 0.1 V
Output	Digital
Microcontroller for auxetic legs control	
Type	AT MEGA 328P
Bit	8 bit
Analog inputs	14 channels
PWM outputs	10 channels
Programmer	Matlab R2021b, MultiWii
Interface software	Arduino IDE
Data rate	115200 bits/s
Control algorithm	SMO-MPC control
Servo motor at auxetic landing gear	
Type	Radio controlled
Torque	35 kg
Accuracy	1.8 °
Sensitivity	5 ms
Signal input	Pulse modulated wave and pulse position modulation
Angular displacement at degrees	0 °–180 °

Figure 6 displays the rotation angle of a drone in degrees over time in seconds, comparing the performance of a standard MPC with that of an SMO-enhanced MPC (SM-MPC). Looking at the past performance, indicated on the left side of the dashed vertical line, both systems exhibit fluctuations around the target angle, with the standard MPC having a maximum overshoot of 20.12 degrees and a downfall of 12.34 degrees. The SMO-MPC shows a more controlled response with less deviation, implying that the SMO tuning has likely improved the MPC's predictive and control horizons. The predictive horizon shows the estimated future behavior of the drone's rotation angle, with the SM-MPC predicting a more stable and controlled future response, suggesting better anticipation of the system's dynamics and potentially more effective control actions to maintain the desired trajectory.

Figure 7(a) shows the control mechanism of the pitch moment during the perched landing. This includes three positions with respect to the pitch angle. It could be observed that the setpoint for the first position of the auxetic foot during perching with 15 deg of angular displacement was controlled over a period of time of 14 seconds. The SMO-MPC obtains a maximum overshoot of 15.4 deg and a downfall of 13.23 deg. In the conventional Model Predictive Control setup, it has been observed that the maximum overshoot is 20.12 degrees, with a subsequent decrease of 12.34 degrees. The second position of the perched landing relies on 16 to 24 seconds with 0 deg pitch angle, the maximum overshoot observed is 1.8 deg and undershoot is -0.5 deg for SMO-MPC. In case of conventional MPC, the overshoot and undershoot are 19 deg and 1 deg, respectively. In the third position, at a time period of 26 to 42 seconds, the highest peak recorded for SMO-MPC is -6.23 and lowest peak is -2.69, while for conventional MPC, the higher and lower pears are -7.98 and -1. The results of tracking the pitch angle are shown in Fig. 7(a). Some ranges of the reference pitch angle do not result in an improved steady-state response. However, adjusting the control horizon in MPC Controllers through proper training enhances setpoint tracking performance.

Figure 7(b) shows how well the yaw angle tracking works. The tracking performance of SMO-MPC is much improved, and the horizons obtained via the SMO-based tuning algorithm are robust. The highest peak observed in SMO-MPC is 1.02 deg, for conventional MPC - 2.7 deg, whereas the lowest peak observed in SMO-MPC is -0.23 deg, for conventional MPC - -1.32 in the time period of 42 seconds.

Figure 7(c) illustrates how modifying the control horizon gains for the control of the roll angle affects the accuracy with

which the roll angle is tracked. Here, the maximum overshoot of 0.65 deg and undershoot of -0.2 deg for SMO-MPC is recorded. In case of conventional MPC, the maximum overshoot observed is 1.98 deg; the undershoot is –0.53 deg in the time period of 42 seconds. Variations in parameters such as uneven surface cause stabilisation problems even while the reference roll angle remains constant. Despite this disturbance, the proposed control mechanism works as intended.

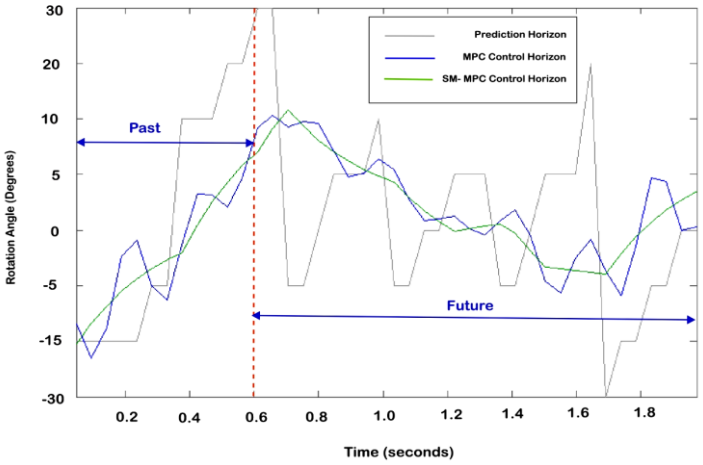

Fig. 6. Landing dynamic control response.

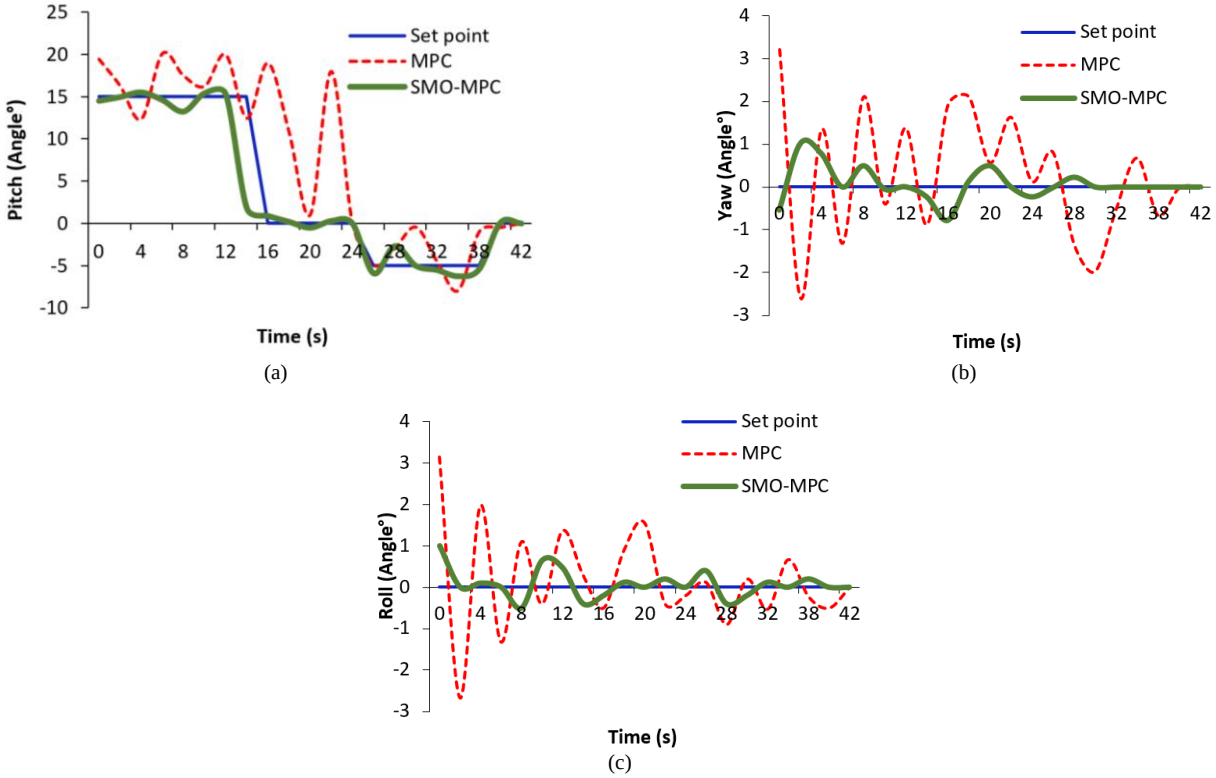

Fig. 7. Landing dynamics of drone with a wind velocity of 4.4 m/s and landing velocity of 0.254 m/s: (a) Effects of variation in pitch angle with respect to landing time using MPC and SMO-MPC; (b) Effects of variation in yaw angle with respect to landing time using MPC and SMO-MPC; (c) Effects of variation in roll angle with respect to landing time using MPC and SMO-MPC.

Based on the data in Fig. 8, it appears that friction forces (auxetic grippers) are superior to torsional forces in terms of stabilising the system. Better landing stability can be achieved by using measures such as adding negative or large positive mechanical trail, applying mass balancing to the landing systems by adjusting the speed of four motors (M1, M2, M3, M4), utilising auxetic dampers (foot of the drone rf, lf), and separating lateral and torsional frequencies via lateral and torsional stiffness modifications. It is inferred from the graph that the damping of landing impact force is higher than that of conventional MPC. The SMO-MPC system exhibits a maximum damping force of 79N and a minimum of 70N, indicating a narrow force range and consistent performance. In contrast, the conventional MPC shows a wider range, with a maximum force of 134N and a minimum of 55N, suggesting a less stable control with greater variability in the damping force applied. Thus, damping the impact force reduces the stress on the internal components of the drone, such as sensors, actuators, and electronics, prolonging their operational lifespan. It also minimises the risk of payload damage and ensures the safety of any cargo or equipment carried by the drone.

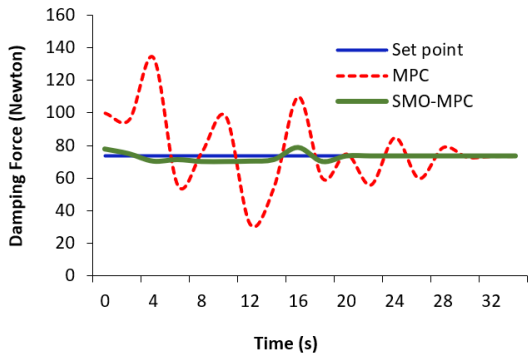

Fig. 8. Control response of MPC and SMO-MPC during setpoint tracking of damping force.

Model predictive control (MPC) is an optimisation-based control technique that helps designers create control strategies and tackle complex drone landing dynamics objectives and limitations [30]. It offers numerous advantages in drone landing dynamics, including handling nonlinear aerodynamics, propulsion systems, and external disturbances [31]. Utilising nonlinear models, MPC optimises nonlinear systems, ensuring accurate and robust landings. It also handles limitations on system states, inputs, and outputs, ensuring drone safety and practicality during landing. The response graph (Fig. 9) shows that the peak time for the SMO-MPC control is 22 s, the rise time is 5 s, and the settling time is 39.45 s. There is less overshoot and more setpoint tracking. While the other control response for the MPC control indicates a peak time of 28 s, rise time of 10 s, and settling time of 55.45 s, the response graph reveals these, respectively. However, the new model is based on heuristic algorithms that have a precise upper bound and lower bound, both of which contribute to the robust stability that was previously lacking in the use of basic models by early predictive controllers [32]. The control horizon (Ch) (as shown in Fig. 6) parameters are selected according to the experimental step responses or the system that generates marginal stability, which results in stable proportional action.

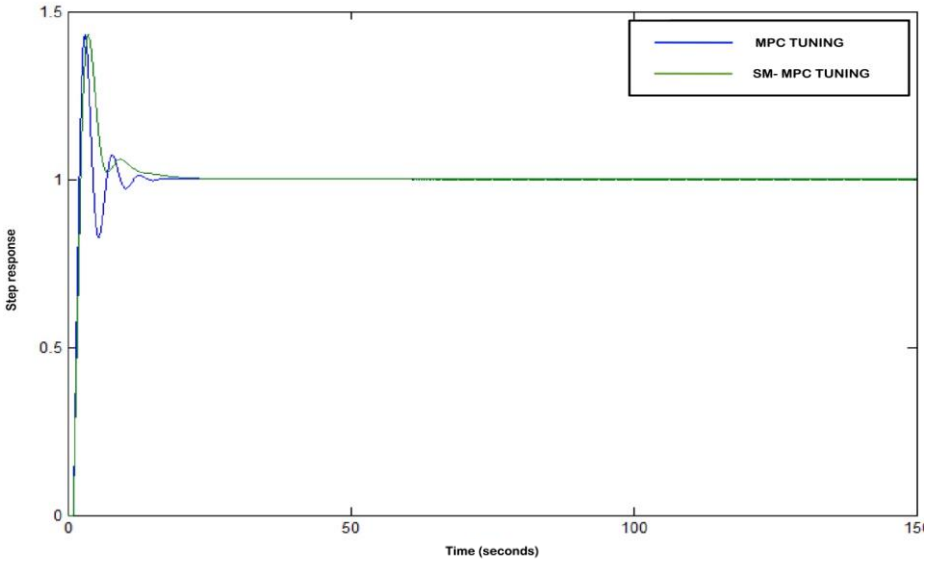

Fig. 9. Step responses of the SMO-MPC and MPC control.

It also handles time-varying control, adjusting control actions to time-varying dynamics for optimal landing performance by prioritising tracking performance and minimising cost functions across a prediction horizon (Ph) (Fig. 6). It is inferred from the above results that the percentage of deviation from the setpoint of MPC for pitch, roll, yaw, and damping force is 29.66 %, 1.6, 1.575, and 86.79, respectively, while the percentage of deviation from the setpoint for SMO-MPC is 3.33, 0.27, 0.5, and 79.7, respectively (Figs. 7(a)–(c)). Table II shows the optimized response outputs of the SMO-MPC with respect to the conventional MPC.

TABLE II. TIME RESPONSE ANALYSIS.

Controller	Rise Time (s)	Overshoot (%)	Peak Time (sec)	Settling Time (s)
MPC	10	1.48	28	55.45
SMO-MPC	5	1.35	22	39.45

The SMO-MPC was found to be robust to model errors, to update predictions based on measurable data during runtime, making it more resilient to model errors, and enhancing landing performance in unpredictable dynamics [20].

VII. CONCLUSIONS AND FUTURE SCOPE

The spider monkey optimisation (SMO)-based model predictive control (MPC) is a promising approach for optimising drone landing gear control, which is crucial for ensuring stability, balance, and impact resistance during landing. The MPC control involves predicting future behaviour and computing control input to optimise the performance criterion over a finite time horizon. The SMO algorithm, inspired by the social behaviour of spider monkeys, provides a global search capability and can escape local optima. Implementing SMO in MPC control improves landing gear control performance, particularly in complex scenarios such as uneven terrain or adverse weather conditions.

The process involves defining the MPC problem, implementing the SMO algorithm, simulating the landing gear system, evaluating its performance, and optimising the parameters of the SMO algorithm.

This optimisation improves the safety and stability of

drone operations. However, the performance of the SMO algorithm depends on carefully tuned parameters, and the computational complexity of the MPC control algorithm may increase, especially for large-scale landing gear systems.

More research is needed to explore its performance in various landing scenarios and optimise parameters for optimal performance. SMO-based MPC has potential applications in autonomous systems, process control, renewable energy systems, aerospace engineering, and biomedical engineering.

ACKNOWLEDGMENT

The authors thank Mr. R. Raj Jawahar Rajan, Research Scholar, Department of Mechanical Engineering, Chennai Institute of Technology, Chennai, India, for his technical support in conducting the experimental work.

CONFLICTS OF INTEREST

The authors declare that they have no conflicts of interest.

REFERENCES

[1] G. Jia, B. Ding, and M. Li, "Mathematical derivation and simulational verification for aggressive quadrotor perching control", in *Proc. of 2021 China Automation Congress (CAC)*, 2021, pp. 5319–5324. DOI: 10.1109/CAC53003.2021.9728145.

[2] A. L. Desbiens and M. R. Cutkosky, "Landing and perching on vertical surfaces with microspines for small unmanned air vehicles", *Journal of Intelligent and Robotic Systems*, vol. 57, no. 1, pp. 313–327, 2010. DOI: 10.1007/s10846-009-9377-z.

[3] A. L. Desbiens, A. T. Asbeck, and M. R. Cutkosky, "Landing perching and taking off from vertical surfaces", *The International Journal of Robotics Research*, vol. 30, no. 3, pp. 355–370, 2011. DOI: 10.1177/0278364910393286.

[4] J. Li and Y. Li, "Dynamic analysis and PID control for a quadrotor", in *Proc. of 2011 IEEE International Conference on Mechatronics and Automation*, 2011, pp. 573–578. DOI: 10.1109/ICMA.2011.5985724.

[5] A. Basci, "Robust Consensus-based Formation Control of a Group of UAV", *Elektron Elektrotech*, vol. 29, no. 4, pp. 4-10, 2023. DOI: 10.5755/j02.eie.34306.

[6] X. Huang, "Design and analysis of retractable structure of new quadrotor landing gear", *Journal of Physics: Conference Series*, vol. 1750, no. 1, art. ID 012022, 2021. DOI: 10.1088/1742-6596/1750/1/012022.

[7] Y.-C. Liang, P.-C. Chin, Y.-P. Sun, and M.-R. Wang, "Design and manufacture of composite landing gear for a light unmanned aerial vehicle", *Applied Sciences*, vol. 11, no. 2, p. 509, 2021. DOI: 10.3390/app11020509.

[8] T. Campi, S. Cruciani, F. Maradei, and M. Feliziani, "Innovative design of drone landing gear used as a receiving coil in wireless charging application", *Energies*, vol. 12, no. 18, p. 3483, 2019. DOI: 10.3390/en12183483.

[9] X. Ni, Q. Yin, X. Wei, P. Zhong, and H. Nie, "Research on landing stability of four-legged adaptive landing gear for multirotor UAVs", *Aerospace*, vol. 9, no. 12, p. 776, 2022. DOI: 10.3390/aerospace9120776.

[10] P. Bauer, "A simple landing gear simulation model for unmanned aerial vehicles", *Periodica Polytechnica Transportation Engineering*, vol. 42, no. 1, pp. 11–18, 2014. DOI: 10.3311/PPtr.7062.

[11] M.-L. Cheng and M. Matsuoka, "Extracting three-dimensional (3D) spatial information from sequential oblique unmanned aerial system (UAS) imagery for digital surface modeling", *International Journal of Remote Sensing*, vol. 42, no. 5, pp. 1643–1663, 2021. DOI: 10.1080/01431161.2020.1842538.

[12] R. Jia, W. Jizhen, L. Xiaochuan, and G. Yazhou, "Terrain-adaptive bionic landing gear system design for multi-rotor UAVs", in *Proc. of 2019 Chinese Control and Decision Conference (CCDC)*, 2019, pp. 5757–5762. DOI: 10.1109/CCDC.2019.8833311.

[13] W. Chu, H. Guo, and W. Xing, "Design of non-similar dual-redundant electromechanical actuation system for UAV landing gear", in *Proc. of 2016 IEEE International Conference on Aircraft Utility Systems (AUS)*, 2016, pp. 592–595. DOI: 10.1109/AUS.2016.7748119.

[14] Z. Qu, W. Chen, J. Zhao, D. Zhang, and G. Zhu, "Simulation of the pneumatic retraction/extension system for UAV landing gear", in *Proc. of CSAA/IET International Conference on Aircraft Utility Systems (AUS 2022)*, 2022, pp. 1152–1157. DOI: 10.1049/icp.2022.1829.

[15] M. Ikura, L. Miyashita, and M. Ishikawa, "Real-time landing gear control system based on adaptive 3D sensing for safe landing of UAV", in *Proc. of 2020 IEEE/SICE International Symposium on System Integration (SII)*, 2020, pp. 759–764. DOI: 10.1109/SII46433.2020.9026177.

[16] T. Muskardin *et al.*, "A novel landing system to increase payload capacity and operational availability of high altitude long endurance UAV", in *Proc. of 2016 International Conference on Unmanned Aircraft Systems (ICUAS)*, 2016, pp. 495–504. DOI: 10.1109/ICUAS.2016.7502668.

[17] M. Magesh, P. K. Jawahar, and SN Saranya, "Spider monkey based metaheuristic tuning of PID controllers for stability landing of UAV's with SMP-auxetic landing gears", in *Proc. of 2022 First International Conference on Electrical, Electronics, Information and Communication Technologies (ICEEICT)*, 2022, pp. 1–6. DOI: 10.1109/ICEEICT53079.2022.9768577.

[18] M. Magesh and P. K. Jawahar, "Examination of shape memory polymer-auxetic landing gears on landing approach for quadcopter", *Materials Today: Proceedings*, vol. 47, part 1, pp. 471–479, 2021. DOI: 10.1016/j.matpr.2021.05.030.

[19] M. Misin and V. Puig, "LPV MPC control of an autonomous aerial vehicle", in *Proc. of 2020 28th Mediterranean Conference on Control and Automation (MED)*, 2020, pp. 109–114. DOI: 10.1109/MED48518.2020.9183041.

[20] T. Zhang, G. Kahn, S. Levine, and P. Abbeel, "Learning deep control policies for autonomous aerial vehicles with MPC-guided policy search", in *Proc. of 2016 IEEE International Conference on Robotics and Automation (ICRA)*, 2015, pp. 528–535. DOI: 10.1109/ICRA.2016.7487175.

[21] L. Jiajin, L. Rui, S. Yingjing, and Z. Jianxiao, "Design of attitude controller using explicit model predictive control for an unmanned quadrotor helicopter", in *Proc. of 2017 Chinese Automation Congress (CAC)*, 2017, pp. 2853–2857. DOI: 10.1109/CAC.2017.8243262.

[22] J. Zhang, X. Xu, and W. Wang, "PWA model based convergence analysis of predictive control system", in *Proc. of the 2006 6th World Congress on Intelligent Control and Automaton*, 2006, pp. 6242–6246. DOI: 10.1109/WCICA.2006.1714283.

[23] A. A. Najm and I. K. Ibraheem, "Nonlinear PID controller design for a 6-DOF UAV quadrotor system", *Engineering Science and Technology, an International Journal*, vol. 22, no. 4, pp. 1087–1097, 2019. DOI: 10.1016/j.jestch.2019.02.005.

[24] N. Bouhabza, K. Kara, and M. L. Hadjili, "PID controllers design for a quadrotor system using teaching learning based optimization", *WSEAS Transactions on Applied and Theoretical Mechanics*, vol. 16, pp. 94–109, 2021. DOI: 10.37394/232011.2021.16.10.

[25] K. Khuwaja, N.-u-Z. Lighari, I. C. Tarca, and R. C. Tarca, "PID controller tuning optimization with genetic algorithms for a quadcopter", *Recent Innovations in Mechatronics*, vol. 5, no. 1, pp. 1–7, 2018. DOI: 10.17667/riim.2018.1/11.

[26] X. Liu, Q. Zhu, and P. Narayan, "Case studies on U state space control system design for quadrotor model", in *Proc. of 2016 8th International Conference on Modelling, Identification and Control (ICMIC)*, 2016, pp. 857–862. DOI: 10.1109/ICMIC.2016.7804234.

[27] P. Tondel, T. A. Johansen, and A. Bemporad, "An algorithm for multi-parametric quadratic programming and explicit MPC solutions", *Automatica*, vol. 39, no. 3, pp. 489–497, 2003. DOI: 10.1016/S0005-1098(02)00250-9.

[28] Y. Lan, Q. Chen, L. Zhang, and R. Long, "Model predictive control based on spider monkey optimization algorithm of interleaved parallel bidirectional DC-DC converter", in *Proc. of 2020 16th International Conference on Control, Automation, Robotics and Vision (ICARCV)*, 2020, pp. 50–55. DOI: 10.1109/ICARCV50220.2020.9305361.

[29] Z. Peng, B. Li, X. Chen, and J. Wu, "Online route planning for UAV based on model predictive control and particle swarm optimization algorithm", in *Proc. of the 10th World Congress on Intelligent Control and Automation*, 2012, pp. 397–401. DOI: 10.1109/WCICA.2012.6357907.

[30] F. Mohseni, E. Frisk, and L. Nielsen, "Distributed cooperative MPC for autonomous driving in different traffic scenarios", *IEEE Transactions on Intelligent Vehicles*, vol. 6, no. 2, pp. 299–309, 2021. DOI: 10.1109/TIV.2020.3025484.

[31] A. Bemporad and D. M. de la Peña, "Multiobjective model predictive control", *Automatica*, vol. 45, no. 12, pp. 2823–2830, 2009. DOI: 10.1016/j.automatica.2009.09.032.

[32] D. Burk, A. Völz, and K. Graichen, "A modular framework for distributed model predictive control of nonlinear continuous-time systems (GRAMPC-D)", *Optimization and Engineering*, vol. 23, no. 2, pp. 771–795, 2022. DOI: 10.1007/s11081-021-09605-3.